# Toward Online Modeling for Lesion Visualization and Monitoring in Cardiac Ablation Therapy

Cristian A. Linte, Jon J. Camp, David R. Holmes III,
Maryam E. Rettmann, and Richard A. Robb

Biomedical Imaging Resource, Mayo Clinic, Rochester, MN, USA
{linte.cristian,robb.richard}@mayo.edu

**Abstract.** Despite extensive efforts to enhance catheter navigation, limited research has been done to visualize and monitor the tissue lesions created during ablation in the attempt to provide feedback for effective therapy. We propose a technique to visualize the temperature distribution and extent of induced tissue injury via an image-based model that uses physiological tissue parameters and relies on heat transfer principles to characterize lesion progression in near real time. The model was evaluated both numerically and experimentally using *ex vivo* bovine muscle samples while emulating a clinically relevant ablation protocol. Results show agreement to within 5°C between the model-predicted and experimentally measured end-ablation tissue temperatures, as well as comparable predicted and observed lesion characteristics. The model yields temperature and lesion updates in near real-time, thus providing reasonably accurate and sufficiently fast monitoring for effective therapy.

## 1 Introduction

Catheter ablation entails the navigation of a percutaneously inserted catheter into the heart and delivery of radio-frequency (RF) energy to induce local tissue necrosis to electrically isolate regions that generate or propagate arrhythmia. Cardiac ablation procedures are conducted under image guidance, where medical imaging, typically X-ray fluoroscopy, is used to guide the catheter to the intracardiac targets [1]. Reported ventures into the treatment of cardiac arrhythmia have been somewhat discouraging, with a fairly high number of patients requiring revisions [2]. We have identified two significant factors that have hampered the success of catheter ablation therapy: inadequate visualization inside the beating heart for accurate targeting of the arrhythmic sites; and lack of effective feedback (i.e., lesion size and tissue injury) on the ablation process.

Visualization in traditional ablation procedures has been impeded by the inherent limitations of X-ray fluoroscopy, mainly arising due to poor visualization of the endocardial surface and requisite catheter contact. Our prior research has addressed the limitations of traditional guidance [3], by developing a novel prototype system for advanced visualization for image-guided cardiac ablation. This platform incorporates pre-operative, patient-specific cardiac models, electro-physiology data acquired via commercial navigation systems, tracked US imaging, and tracking of the ablation catheter.

K. Mori et al. (Eds.): MICCAI 2013, Part I, LNCS 8149, pp. 9–17, 2013.

The other critical factor to successful ablation, which we address here, is intra-operative feedback on the quality of the delivered lesions. While several groups have developed mathematical and physiological models [1] to investigate lesion development in response to RF energy delivery [4,5] for cardiac ablation, to our knowledge, little effort has been channeled toward the integration of such models into the clinical workflow, to visualize and monitor tissue injury, and avoid incomplete electrical pathway isolation during ablation. The slow progress has primarily been attributed to the challenge of developing sufficiently fast ablation models capable of computing temperature distribution and lesion progression in real time [6].

To complement our navigation platform with simultaneous online therapy monitoring [7,8], here we propose a fast and reasonably accurate surrogate ablation model that provides estimates of temperature distribution, tissue damage and lesion progression. The cardiologist will have access to a dynamic visual display of "ablation lesion maps" consisting of sequentially created lesions, rather than just a glyph indicating the catheter location, which can be used to guide the delivery of subsequent lesions to ensure suppression of arrhythmia.

## 2 Materials and Methods

### 2.1 Ablation Model

The tissue response to RF energy can be approximated with sufficient accuracy by a coupled resistive - conductive heat transfer process [1]. The proposed surrogate ablation model incorporates a resistive component occurring at the electrode-tissue interface, and a conductive component responsible for the energy diffusion into the tissue. The heat transfer equilibrium equation the tissue during ablation is governed by the bioheat equation [9]:

$$\rho \cdot c \cdot \frac{\partial T}{\partial t} \;=\; \nabla \cdot (k \nabla T) \;+\; q \;-\; Q_p \;+\; Q_m \tag{1}$$

where $\rho$ is the density ($kg/m^3$), $c$ is the specific heat ($J/kg{\cdot}K$), $k$ is the thermal conductivity ($W/m \cdot K$); $Q_p$ is the perfusion heat loss ($W/m^3$) — typically neglected for cardiac ablation [10], $Q_m$ is the metabolic heat generation ($W/m^3$), which was shown to be insignificant [11,12], and, lastly, $q$ is the heat source ($W/m^3$), representing the energy deposited into the tissue within a small radius around the electrode and approximated by a purely resistive, quasi-static Joule heating.

**Model Formulation and Image-Based Implementation:** The ablation electrode is represented by a virtual construct based on the physical properties of the electrode, and its interaction with the tissue is defined by means of voxel occupancy in the image volume. The delivered power is absorbed within the first 1-1.5 mm from the electrode surface. During clinical procedures, energy is gradually delivered to the tissue up to a set level (30-50W), then modulated to maintain the electrode temperature at a preset value [13] (typically

60°C - 90°C). The temperature control is modeled according to the gradient between the preset target and the dynamically updated electrode-tissue interface temperature, and modulates power delivery to maintain the target temperature. Tissue voxels remote from the catheter receive energy via heat conduction, modeled as isotropic diffusion. Tissue thermal conductivity has been traditionally treated as a constant parameter with a nominal value of 0.51 - 0.59 $W/m \cdot K$ for myocardium [14], while the other physiological parameters used in the model are assigned literature-suggested values [15]: as follows ($\rho_{blood} = 1000kg/m^3$, $\rho_{tissue} = 1070kg/m^3$, $c_{blood} = 4180J/kg \cdot K$, and $c_{tissue} = 3500J/kg \cdot K$). The endocardial blood flow is modeled by maintaining the blood pool voxels at 37°C.

Our proposed ablation model follows an image-based implementation, using an anatomical 3D image (i.e., a patient-specific cardiac CT or MR) labeled as blood and tissue compartments, with assigned physiological parameters. The following *image volumes* are used to predict tissue temperature, extent of tissue damage, and lesion progression during ablation: a *conductivity volume* is generated by assigning each image compartment (i.e., tissue and blood pool) the appropriate conductivity values; an image volume of the tissue region is initialized to 37°C and labeled as the initial tissue *temperature volume*; a tissue *exposure volume* is generated based on the cumulative "exposure" (i.e., area under the temperature-time curve explained later) of each voxel in the tissue *temperature volume*; lastly, a tissue *lesion volume* is generated by digitally marking voxels in the tissue *exposure volume* as either irreversible lesion if exposed to 55°C or above for at least 5 s, or reversible lesion penumbra otherwise.

**Tissue Damage and Lesion Characterization:** Modeling studies have used the 50°C isotherm to assess tissue damage reversibility — tissue rendered nonviable after ablation could be defined by the volume enclosed by the 50°C isothermal surface [16]. However, since tissue damage is a function of temperature and time [6], we define *cumulative exposure* as a measure of induced tissue injury.

Cumulative exposure is the area under the temperature-time curve calculated on a voxel-basis over the duration of the ablation: $E = \int_0^{t_{cell-death}} T(t)\ dt\ + \int_{t_{cell-death}}^{t_{max}} T(t)\ dt$, where $t_{cell-death}$ is the time at which a voxel has reached the cell-death temperature ($T_{cell-death} = 55°C$). The former term represents the voxel exposure prior to reaching cell-death temperature (i.e., reversible damage and lesion penumbra), while the latter term represents the voxel exposure beyond cell-death temperature for 5 s or longer (i.e., irreversible damage and core lesion).

A more traditional approach for quantifying tissue injury follows an Arrhenius relationship [17]: $\Omega(t) = \int_0^t P \cdot e^{\frac{-\Delta E}{R \cdot T}}\ dt$, where $T$ is the voxel tissue temperature (K), $R$ is the universal gas constant, and P ($s^{-1}$) and $\Delta E$ ($J/mole$) are tissue specific kinetic coefficients evaluated experimentally [18] and validated against RF ablation experiments [12]. Tissue damage accumulates linearly with time and hyperbolically with temperature, rendering tissue injury as reversible for $\Omega < 0.5$, and irreversible for $\Omega > 1.0$. As demonstrated in section **3**, both the Arrhenius and the 50°C isotherm tissue injury criteria yield consistent results with our proposed exposure criterion, yet at a higher computational expense.

### 2.2 Numerical Model Evaluation

We conducted numerical experiments to assess model behaviour in response to several parameters, including tissue damage criteria, electrode-tissue contact, and also simulated a cooled vs. dry electrode ablation, as shown in section **3**.

### 2.3 *Ex vivo* Experimental Evaluation

To validate our model we conducted a series of *ex vivo* ablation experiments. Bovine muscle samples (1-cm thick) were submerged in a 0.9% saline bath. Endocardial blood flow was mimicked using an immersion circulator (6 L/min flow-rate) that maintained the saline at 36±0.5°C. A RF power generator (Boston Scientific, Natick, MA) was used to deliver energy via a non-cooled 9F 4 mm electrode. The catheter was depressed into the tissue by 1.5 mm, to achieve firm hemispherical contact. The generator was operated in temperature-control mode at 90°C target temperature and 40W maximum power level. Direct tissue temperature measurements, considered as ground truth, were recorded using focal 0.8 mm dia. fiberoptic temperature probes inserted at specific tissue locations.

## 3 Model Evaluation and Results

**Tissue Damage Criteria:** We compared the extent of injury characterized according to our tissue exposure formulation (irreversible damage above 55°C for 5s or longer), to the Arrhenius (irreversible for $\Omega > 1.0$), and 50°C isotherm damage criteria. As shown in **Fig. 1**, the size of the irreversibly-damaged region predicted by the voxel exposure criterion is within 1 mm diameter difference from the region predicted by the Arrhenius and 50°C isotherm criteria.

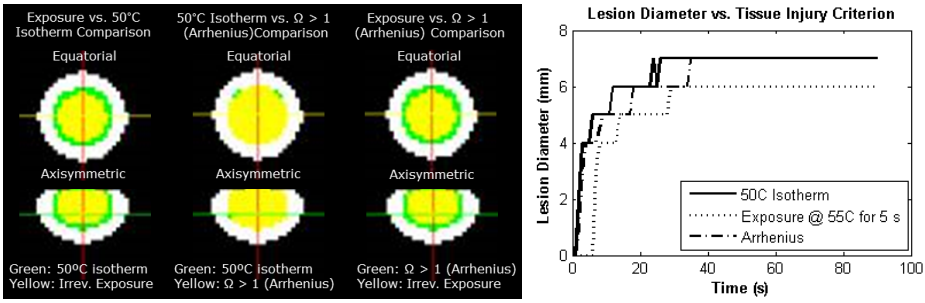


**Fig. 1.** Comparison of the irreversible region assessed according to the three injury criteria. Irreversible lesion diameter predicted by the injury criteria: the voxel exposure criterion leads to lesion diameter within 1 mm of that assessed according to the Arrhenius and 50°C isotherm injury criteria.

**Electrode-Tissue Contact:** The extent of electrode-tissue contact is a direct indicator of the lesion size [19]. We address electrode-tissue contact by modeling three different cases of electrode penetration depth, and asses the outcome according to the achieved lesion dimension as illustrated in **Fig. 2**.

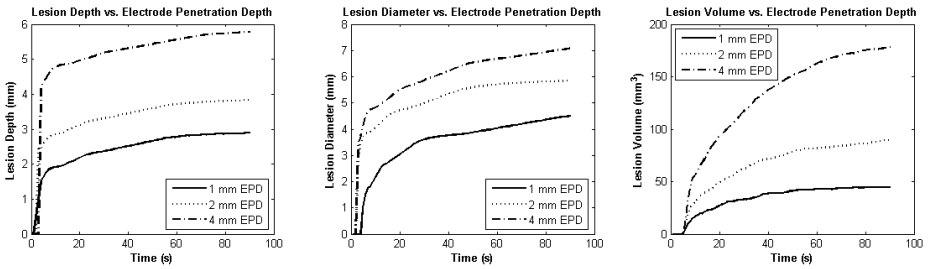


**Fig. 2.** Model-predicted lesion depth, diameter and volume as a result of increasing electrode-penetration depth (1, 2 and 4 mm). Observed trends (larger lesions with deeper penetration) are consistent with previous simulation results reported in [20].

**Cooled vs. Dry Electrode Ablation:** In addition to modeling traditional ablation catheters with no active cooling, we employed the approximation adopted in [21,22] to model a cooled ablation procedure and assessed its effects by characterizing the resulting lesion. Cooling was modeled by setting a lower temperature boundary condition at the electrode surface equal to the temperature of the cooling fluid. This first order approximation will be improved by allowing heat exchange between the electrode and tissue. **Fig. 3** shows the model-predicted tissue temperature at the end of 90-second ablation procedures, with no electrode

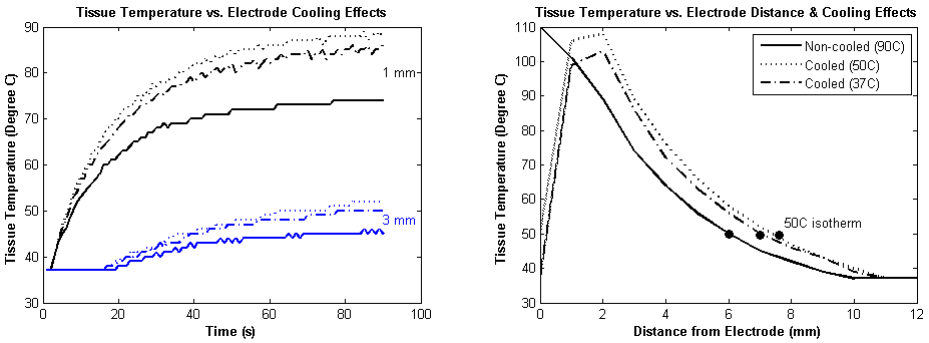


**Fig. 3.** End-ablation tissue temperature at 1 and 3 mm from electrode tip during a non-cooled, 90°C temperature-controlled ablation, as well as two cooled ablations at 50°C and 37°C. Cooling leads to the shift of the 50°C isotherm from $\sim$ 6 mm to $\sim$ 8 mm. These findings agree with [22] — electrode cooling shifts the hot spots away from the electrode resulting in deeper lesions.

**Table. 1.** Model-predicted and experimentally measured tissue tissue temperature distribution during 60 s ablation at 90° C

| Time Stamp (sec) | Proximal Lesion Location | | Distal Lesion Location | |
|---|---|---|---|---|
| | Measured Temp. (°C) | Predicted Temp. (°C) | Measured Temp. (°C) | Predicted Temp. (°C) |
| 11.2 | 68.9 ± 4.9 | 63.8 | 37.2 ± 1.7 | 37.1 |
| 19.6 | 73.0 ± 5.2 | 70.7 | 39.0 ± 1.6 | 37.9 |
| 30.8 | 76.2 ± 4.8 | 74.9 | 39.8 ± 2.3 | 38.7 |
| 39.2 | 77.4 ± 5.3 | 77.2 | 40.6 ± 2.6 | 40.3 |
| 50.4 | 78.7 ± 5.4 | 78.8 | 40.9 ± 3.2 | 41.2 |
| 58.8 | 79.1 ± 4.9 | 78.9 | 41.5 ± 3.4 | 42.3 |

**Table. 2.** Model-predicted lesion characterization parameters during 60 s ablation at 90° C

| Time Stamp (sec) | Lesion Volume ($mm^3$) | Maximum Lesion Dia. (mm) | Surface Lesion Dia. (mm) | Surface Exposure Dia. (mm) |
|---|---|---|---|---|
| 5 | 30.2 | 3.8 | 4.0 | 7.6 |
| 10 | 44.1 | 4.2 | 4.5 | 8.3 |
| 20 | 63.1 | 4.8 | 4.8 | 8.6 |
| 30 | 77.5 | 5.2 | 4.9 | 9.0 |
| 40 | 84.5 | 5.6 | 4.9 | 9.1 |
| 60 | 96.0 | 5.8 | 5.0 | 9.4 |

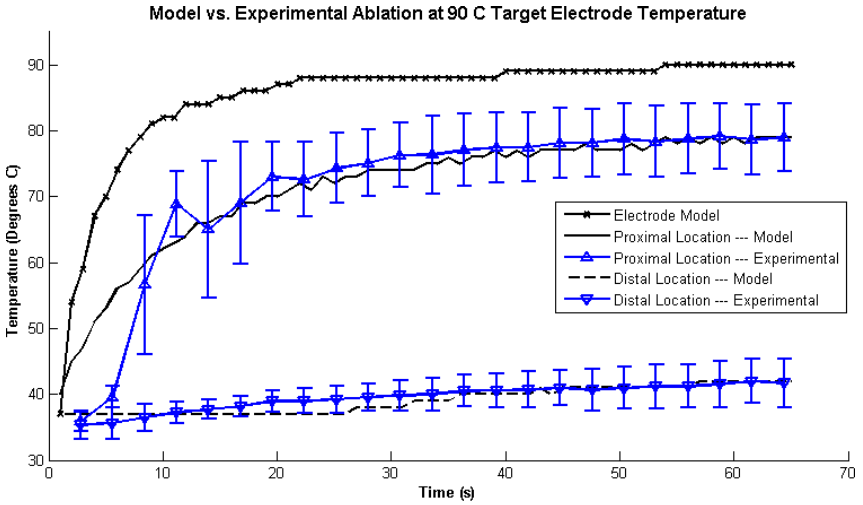


**Fig. 4.** Time-varying temperature plots of the electrode model, as well as model-predicted and experimentally-measured (Mean ± Std. Dev.) temperatures at the proximal and distal locations

cooling (90°C ablation), and two cooled ablations at 50°C and 37°C. The cooling effect led to higher tissue temperatures at both locations, and contributed to the shift of the temperature distribution deeper within the tissue.

**Experimental Model Evaluation:** Four fiberoptic temperature probes were inserted into the tissue samples in a symmetric pattern relative to the ablation electrode at specified radial distance (R) and depth (D); two probes measured tissue temperature at 2.5 mm R x 3 mm D from the electrode (proximal location), and two probes measured temperature at 5 mm R x 3 mm D (distal location). Measurements were recorded simultaneously from all temperature probes and experiments were repeated three times on fresh tissue samples.

**Table 1** and **Fig. 4** summarizes the tissue temperature distribution at the two lesion locations, showing agreement within 5°C between the model-predicted and experimentally recorded temperatures.

The modeled lesions were characterized according to lesion volume, maximum diameter, surface lesion diameter, and surface exposure diameter, summarized in **Table 2**. After the experiments, the samples were analyzed according to the diameter and depth of the region marked by tissue discolouration, also known to correspond with the volume enclosed by 50°C isothermal surface [6]. The lesion measurements predicted by the model were consistent with those observed in the digital images of the post-ablation samples (**Fig. 5**).

**Fig. 5** also shows 2D cross-sectional renderings of the model-generated lesion at 5, 10, 30, and 60 s during the ablation. The irreversibly damaged tissue region appears brighter and is surrounded by the lesion penumbra.

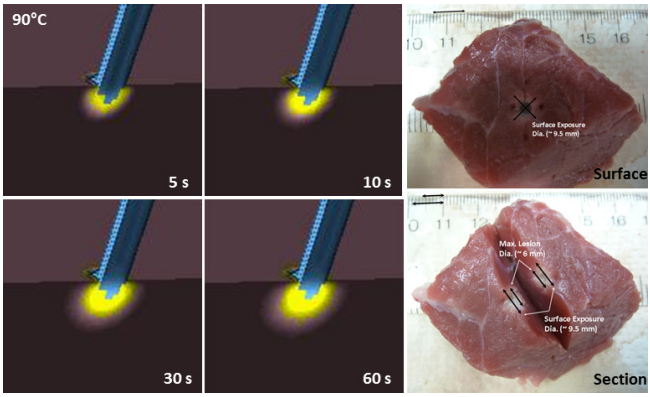


**Fig. 5.** Cross-sectional rendering of the model-predicted tissue damage at four time points during 90°C ablation. Note the irreversibly damaged region appearing bright and surrounded by the lesion penumbra. Post-ablation digital images of a typical sample following 90°C ablation: a surface exposure diameter of $\sim$ 9 mm and a maximum lesion diameter of $\sim$ 6 mm shown in the section, both consistent with the model-predicted dimensions.

## 4 Discussion

We describe the development, implementation, and evaluation of an image-based ablation model designed to assist with procedure guidance and provide visualization and monitoring of lesion progression during RF ablation. Given the real-time guidance requirement and the understanding of clinically acceptable accuracy, this model is not intended to provide the computational rigor of previously developed finite element models of tissue ablation; it is rather a "surrogate" model that demonstrates effective and fast extension of a theoretical model into a practical tool, designed for efficient intra-operative integration with our navigation platform for image-guided cardiac ablation therapy.

We explored the effect of electrode penetration depth as a contact surrogate, electrode cooling, and also compared our exposure tissue injury criterion to two other criteria explored in the literature. Numerical experiments confirmed previous findings, while the experimental studies also demonstrated agreement within 5°C between the model-predicted and experimentally measured temperature profiles. Lastly, the predicted and observed lesion patterns were also in agreement, suggesting sufficiently accurate modeling of the ablation process.

In its current form, the model is implemented using a 0.5 mm isotropic image substrate, which is inline with the typical resolution of clinical-quality acquired images, as well as the 1.0-2.0 mm accuracy of the magnetic tracking system used to identify the position and pose of the ablation catheter.

The proposed model was implemented on a standard desktop PC (Intel Core2 Quad 2.5 GHz, 8 GB DDR2 RAM) and provided near real-time updates of the tissue temperature distribution and lesion progression. modeling a 60s ablation cycle in $\sim$ 1 minute The computational efficiency can be further improved via parallel multi-thread computing and GPU implementation, enabling lesion monitoring with minimal workflow latency.

Once integrated within the prototype guidance and navigation platform for left atrial ablation therapy, the thermal model will provide the cardiologist with online visualization and monitoring of the changes induced in the tissue during RF energy delivery. In addition to the catheter navigation information available from the image guidance environment (i.e., the tracked catheter tip dictates the location where the ablation lesion should be displayed), the physiological changes occurring in the tissue will be displayed by means of temperature colour maps superimposed on the pre-operative anatomical model, thereby providing improved guidance for the delivery of subsequent lesions.

## 5 Conclusions and Future Work

Given the support provided by new methodologies of planning, simulation and training, the proposed ablation model demonstrates effective and fast extension of a theoretical model into a practical tool that will allow for quantitative monitoring of individual ablation therapy with integrated guidance [8,23].

Knowledge of the true ablation sites and their characterization as necrotic or endemic via DCE-MRI [24] is of significant importance for the *in vivo* validation of the thermal model. As such, future efforts will focus on estimating electrode-tissue interaction and contact using the system-integrated real-time US imaging, as well as evaluating the predicted lesions and guidance abilities of the enhanced system *in vivo* against post-procedural assessment of lesion development as characterized using delayed contrast-enhanced (DCE)-MR imaging, as well as post-mortem using tissue staining techniques.

## References

1. Haemmerich, D.: Crit. Rev. Biomed. Eng. 38(1), 53–63 (2010)
2. Pappone, C., et al.: Circ. 102, 2619–2628 (2000)
3. Rettmann, M.E., et al.: Comput. Methods Programs Biomed. 95, 95–104 (2009)

4. Pearce, J.A.: Crit. Rev. Biomed. Eng. 38(1), 1–20 (2010)
5. Payne, S.J., et al.: Crit. Rev. Biomed Eng. 38(1), 21–30 (2010)
6. Berjano, E.J.: Biomed. Eng. Online. 18, 5–24 (2006)
7. Johnson, P.C., et al.: Ann. Biomed. Eng. 30, 1152–1161 (2002)
8. Villard, C., et al.: Comput. Methods Biomech. Biomed. Engin. 8, 215–227 (2005)
9. Pennes, H.H.: J. Appl. Physiol. 85, 5–34 (1948)
10. Haines, D.E., et al.: Pacing Clin. Electrophysiol. 12, 962–976 (1989)
11. Chang, I.A., et al.: Biomed. Eng. Online. 3, 1–19 (2004)
12. Labonté, S.: IEEE Trans. Biomed. Eng. 41, 108–115 (1994)
13. Jain, M.K., et al.: IEEE Trans. Biomed. Eng. 46, 1405–1412 (1999)
14. Holmes, K.R.: http://www.ece.utexas.edu/~valvano/research/Thermal.pdf
15. Shahidi, A.V., et al.: IEEE Trans. Biomed. Eng. 41, 963–968 (1994)
16. Panescu, D., et al.: IEEE Trans. Biomed. Eng. 42, 879–890 (1995)
17. Diller, K.R., et al.: Ann. NY Acad. Sci. 888, 153–165 (1999)
18. Pearce, J.A., et al.: Proc. IEEE Eng. Med. Biol. Conf., 256–258 (1998)
19. Yokoyama, K., et al.: Circ. Arrhythm. Electrophisiol. 1(5), 354–362 (2008)
20. Jain, M.K., et al.: Proc. IEEE Eng. Med. Biol. Conf., 245–247 (1998)
21. Berjano, E.J., et al.: Proc. IEEE Eng. Med. Biol. Cong., 2496–2498 (1997)
22. Jain, M.K., et al.: Proc. IEEE Eng. Med. Biol. Conf., 273–274 (1995)
23. Banovac, F., et al.: Med. Phys. 32(5), 2698–2705 (2005)
24. Knowles, B.R., et al.: IEEE Trans. Biomed. Eng. 57, 1467–1475 (2010)